ACS OMEGA

Article

http://pubs.acs.org/journal/acsodf

Gadolinium-Functionalized Peptide Amphiphile Micelles for Multimodal Imaging of Atherosclerotic Lesions

Sang Pil Yoo,[†] Federico Pineda,[‡] John C. Barrett,[†] Christopher Poon,[§,∥] Matthew Tirrell,[†] and Eun Ji Chung*[,†,∥]

[†]Institute for Molecular Engineering, University of Chicago, 5747 South Ellis Avenue, Chicago, Illinois, 60637, United States
[‡]Department of Radiology, University of Chicago, 5841 South Maryland Avenue, MC2026, Chicago, Illinois 60637, United States
[§]Department of Chemistry, University of Chicago, 929 E. 57th Street, Chicago, Illinois 60637, United States

Supporting Information

ABSTRACT: The leading causes of morbidity and mortality globally are cardiovascular diseases, and nanomedicine can provide many improvements including disease-specific targeting, early detection, and local delivery of diagnostic agents. To this end, we designed fibrin-binding, peptide amphiphile micelles (PAMs), achieved by incorporating the targeting peptide cysteine-arginine-glutamic acid-lysine-alanine (CREKA), with two types of amphiphilic molecules containing the gadoliniuim (Gd) chelator diethylenetriamine-pentaacetic acid (DTPA), DTPA-bis(stearylamide)(Gd), and 1,2-distearoyl-*sn*-glycero-3-phosphoethanolamine-*N*-[(poly(ethylene glycol) (PEG))-2000]-DTPA(Gd) (DSPE-PEG2000-DTPA(Gd)). The material characteristics of the resulting nanoparticle diagnostic probes, clot-binding properties in vitro, and contrast enhancement and safety for dual, optical imaging−magnetic resonance imaging (MRI) were evaluated in the atherosclerotic mouse model. Transmission electron micrographs showed a homogenous population of spherical micelles for formulations containing DSPE-PEG2000-DTPA(Gd), whereas both spherical and cylindrical micelles were formed upon mixing DTPA-BSA(Gd) and CREKA amphiphiles. Clot-binding assays confirmed DSPE-PEG2000-DTPA(Gd)-based CREKA micelles targeted clots over 8-fold higher than nontargeting (NT) counterpart micelles, whereas no difference was found between CREKA and NT, DTPA-BSA(Gd) micelles. However, in vivo MRI and optical imaging studies of the aortas and hearts showed fibrin specificity was conferred by the peptide ligand without much difference between the nanoparticle formulations or shapes. Biodistribution studies confirmed that all micelles were cleared through both the reticuloendothelial system and renal clearance, and histology showed no signs of necrosis. In summary, these studies demonstrate the successful synthesis, and the molecular imaging capabilities of two types of CREKA-Gd PAMs for atherosclerosis. Moreover, we demonstrate the differences in micelle formulations and shapes and their outcomes in vitro versus in vivo for site-specific, diagnostic strategies, and provide the groundwork for the detection of thrombosis via contrast-enhancing agents and concurrent therapeutic delivery for theranostic applications.

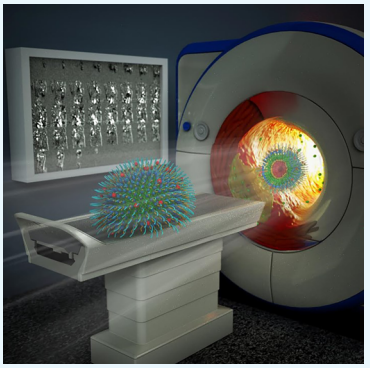

INTRODUCTION

Atherosclerosis contributes to cardiovascular diseases, the leading cause of morbidity and mortality in the United States.[1] Atherosclerosis is characterized as a chronic, inflammatory disease, and its progression is typically slow and asymptomatic until a clinical event occurs such as a myocardial infarction or stroke.[2−4] Many patients who die from sudden cardiac arrest have no prior reports or symptoms of their underlying disease. Current imaging modalities for atherosclerosis diagnostics use imaging techniques that focus on the severity of the blockage within arteries. However, the majority of plaques that rupture occlude <50% of the vessel diameter.[5] Therefore, early detection of unstable plaques is needed and requires imaging techniques that provide information on plaque composition and not just based on size alone.

Magnetic resonance imaging (MRI) is an important imaging modality for vascular occluding diseases.[6] A variety of approaches to detect vulnerable plaques in atherosclerosis have emerged, but the main advantages of MRI as compared to conventional techniques such as computed tomography, X-ray angiography, and intravascular ultrasound is its ability to image and characterize the blood vessel wall and plaque in a noninvasive manner. Moreover, MRI avoids patient's exposure to ionizing radiation, limiting possible long-term health implications. Nonetheless, whereas MRI has the ability to image and generate contrast between health and diseased soft tissues based on $T1$ and $T2$ relaxation times and proton density (PD), contrast-enhanced MRI methods can better discriminate vulnerable plaques by accumulating contrast agents in the diseased vessel wall without significantly enhancing normal vessels.

Received: August 26, 2016
Accepted: November 9, 2016
Published: November 21, 2016

DOI: 10.1021/acsomega.6b00210
ACS Omega 2016, 1, 996−1003

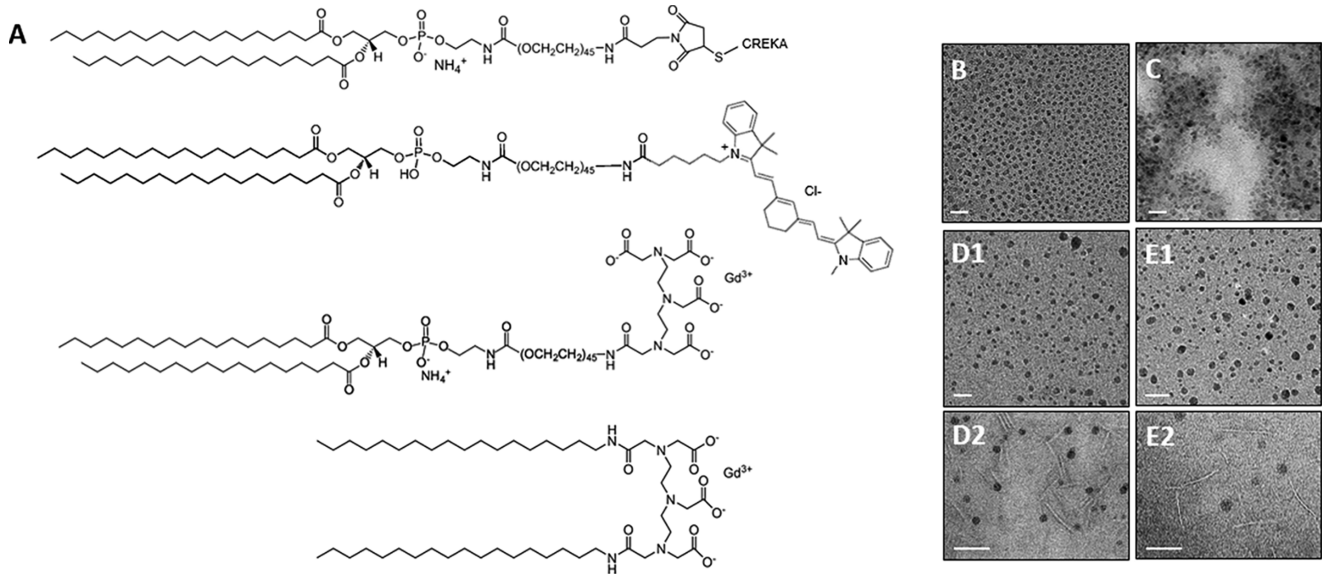

Figure 1. Molecular structure of (A) DSPE-PEG2000-CREKA (top), DSPE-PEG2000-cy7, DSPE-PEG2000-DTPA(Gd), DTPA-BSA(Gd) (bottom). Transmission electron microscopy (TEM) images of (B) CREKA/DSPE-PEG2000−DTPA(Gd), (C) NT/DSPE-PEG2000-DTPA(Gd), (D1) spherical population of CREKA/DTPA-BSA(Gd), (E1) spherical population of NT/DTPA-BSA(Gd), (D2) cylindrical population of CREKA/DTPA-BSA(Gd), and (E2) cylindrical population of NT/DTPA-BSA(Gd). SB: 20 nm (B−E1), 100 nm (D2, E2).

Recent developments in nanomedicine and molecular engineering have improved the design of contrast agents by incorporating molecular targeting ability to disease pathology, as well as strategies to enhance half-life while minimizing toxicity.[7] Specifically, peptide-based nanomaterials are particularly useful for these applications as the peptide is often a biological epitope for tissue-specific homing, with inherent biocompatible and biodegradable characteristics.[8−10] To that end, we have previously incorporated the fibrin-targeting peptide, cysteine-arginine-glutamic acid-lysine-alanine (CREKA), previously found through in vivo phage display, into supramolecular, peptide amphiphile micelles (PAMs) for targeting unstable, atherosclerotic plaques displaying microthrombi.[11−14] Rupture of unstable plaques, presaged by the appearance of microthrombi, leads to activation of thrombin, fibrin deposition, and ultimately occluding clots.[15] Imaging vessels in which clotting is taking place has the potential to enable intervention and reduction of blood vessel occlusion and expansion of clots through preventative therapies.

Individual peptide amphiphile (PA) molecules consist of a hydrophilic, peptide "head group" and a lipid, alkyl "tail", which self-assemble above its critical micelle concentration (CMC) via hydrophobic forces.[16,17] PAMs can include a poly(ethylene glycol) (PEG) protective shell between the peptide and aliphatic tail that provides pharmacokinetic properties favorable for enhanced bioavailability, and deliver contrast agents and drugs in the optimum dosage range, reducing toxic side effects.[18−20] Moreover, notable characteristics of PAMs include their multivalent display of peptides presented on the exterior and multifunctionality through the combination of several amphiphilic monomers, advantages for targeted, diagnostic applications.[11,21]

Our earlier studies in the apolipoprotein E-deficient (ApoE KO) murine model confirmed that CREKA-PAMs accumulate in the shoulder region of late-stage plaques, a region where fibrin deposition and microthrombi are present and most likely to rupture, and are mostly cleared out of the body within a week without adverse effects.[11,12] This is an important aspect to contrast agent development because recent reports have found deposits of contrast agents accumulated in the brain of cadaver patients with repeated imaging, spurring FDA investigation for safety.[22] Through targeting, less contrast agents can be used overall, providing a safer tool particularly for such patients.

To incorporate the molecular targeting ability of PAMs and the diagnostic performance of MRI, the objective of this study is to develop micelles that can be utilized as molecular MRI contrast agents for plaque localization and visualization using *T*1-weighted imaging for atherosclerosis. We synthesized and combined two types of amphiphilic molecules containing the gadoliniuim (Gd) chelator diethylenetriaminepentaacetic acid (DTPA) into CREKA-PAMs: one molecule that is commercially available and previously incorporated into other micelle-based MRI systems (DTPA-BSA(Gd))[23] and another synthesized for the first time and consisting of the 1,2-distearoyl-*sn*-glycero-3-phosphoethanolamine-*N*-(PEG)-2000 (DSPE-PEG2000) backbone (DSPE-PEG2000-DTPA(Gd)). Gd-based MRI contrast agents typically fall into two groups: linear Gd(III) chelates and macrocyclic chelates. Macrocyclic chelates have higher thermodynamic and kinetic stability than that of linear chelates and so we chose DTPA-Gd as the macrocyclic chelator in both instances.[24] Whereas previous studies have incorporated commercially available gadolinium chelators into nanoparticles, we show, for the first time, DTPA(Gd) within the DSPE-PEG2000 backbone of CREKA-PAMs, and provide structural data as well as comparisons between the nanoparticles consisting of varying Gd-amphiphilic molecules regarding targeting in vivo. The novel design and synthesis of combining gadolinium, optical imaging probes, and targeting ligands in PAMs for MRI applications are provided as well as comparisons between nanoparticles, an important aspect to designing particles for clinical translation. We evaluated the material characteristics and relaxivity measurements for MRI feasibility, tested and compared fibrin-targeting capabilities in vitro, and demonstrate contrast enhancement and safety of both micelles as contrast agents in the atherosclerotic mouse model.

DOI: 10.1021/acsomega.6b00210
ACS Omega 2016, 1, 996−1003

RESULTS AND DISCUSSION

Preparation, Characterization, and Comparison of Fibrin-Binding PAMs for MRI. Two types of fibrin-binding PAMs for MRI were self-assembled, one of which was mixed with DTPA-BSA(Gd) (commercially available) and another with DSPE-PEG2000-DTPA(Gd) (Figure 1A). DSPE-PEG2000-DTPA(Gd) was obtained by reacting diethylenetriamine-*N*,*N*,*N*″,*N*″-tetra-*tert*-butyl acetate-*N*′-acetic acid (DTPA-tetra) to DSPE-PEG(2000)-amine to form a peptide bond. The *tert*-butyl groups of DSPE-PEG2000-DTPA-tetra were deprotected and Gd ions were chelated onto the amphiphile by adding $Gd(Cl_3)$. Free Gd ions were separated by a desalting column, and all molecules were purified after each step and confirmed by matrix-assisted laser desorption ionization time-of-flight (MALDI-TOF)/TOF mass spectrometry (Figure S1). A total of four types of micelles were constructed: (1) CREKA/DSPE-PEG2000-DTPA(Gd), (2) nontargeting (NT)/DSPE-PEG2000-DTPA(Gd), (3) CREKA/DTPA-BSA(Gd), and (4) NT/DTPA-BSA(Gd). All micelles consisted of 45:45:10 mol % DSPE-PEG2000-CREKA, DSPE-PEG2000-methoxy/DSPE-PEG2000-DTPA(Gd), or DTPA-BSA(Gd)/DSPE-PEG2000−cy7 to maximize targeting capabilities, MRI contrast, and fluorophore signal. The optimal concentration for PAMs was previously determined to be 10 mol % cy7 without quenching the fluorescence signal.,[20]

Spherical micelles with an average diameter of 8.7−12.4 nm was confirmed via TEM and dynamic light scattering (DLS) (Figure 1B−E2 and Table 1). Upon sterile filtering (0.1 μm, poly(vinylidene difluoride) (PVDF)), TEM confirmed the presence of a heterogeneous population of micelles consisting of both spherical and cylindrical micelles for PAMs consisting of DTPA-BSA(Gd) (Figure S2). DTPA-BSA(Gd) micelles also had a larger population of particles (Figure S3), likely reflecting the cylindrical micelles present in solution. This was also the case for CREKA-PAMs consisting of DSPE-DTPA(Gd), another commercially available chelator (Figure S4). In addition to charge repulsion, DTPA-BSA(Gd) and DSPE-DTPA(Gd) lacks the PEG_{45} linker, which contributes to the larger hydrophilic head group found in DSPE-PEG2000-based amphiphiles and the packing parameter that dictates spherical shape, which may explain these observations.[17] Notably, the apparent darkness of the electron micrographs showed variability in all cases, suggesting that the amount of DTPA(Gd)-containing molecules also varied. The cylindrical micelles derived from DTPA-BSA(Gd)-containing mixtures were lighter in appearance, suggesting less Gd incorporation.

When PAMs were constructed with various DSPE-PEG(2000)-CREKA to DTPA(Gd) molar ratios, an increase in Gd led to a decrease in *T*1 measurements at 1.5 T,[25] confirming the tunability of % Gd incorporation and contrast-enhancing properties of PAMs for MRI (Table 2). An anomaly to this trend are the longitudinal relaxation times for PAMs consisting of >75 mol % Gd for DTPA-BSA-based micelles, in which there was an increase. This phenomenon may be due to the distance of paramagnetic ions to one another within micelles as reported for other nanoparticles.[26,27] *T*1 measurements of micelles were similar to that of water without the presence of Gd.[28]

Table 1. Hydrodynamic Diameter of Micelles

micelle (%)	size (nm)
CREKA/DSPE-PEG2000-DTPA(Gd) (50/50)	10.1 ± 1.5
NT/DSPE-PEG2000-DTPA(Gd) (50/50)	8.7 ± 1.4
CREKA/DTPA-BSA(Gd) (50/50)	9.9 ± 1.7
NT/DTPA-BSA(Gd) (50/50)	12.4 ± 1.2

Table 2. *T*1 Measurements of Micelles with Varying Gd Content at 1.5 T

micelle composition	*T*1 (ms)
CREKA/DSPE-PEG2000-DTPA(Gd)	
100/0	2278 ± 10.5
75/25	1998 ± 8.3
50/50	1580 ± 6.1
25/75	897 ± 7.0
NT/DSPE-PEG2000-DTPA(Gd)	
100/0	2485 ± 6.3
75/25	2187 ± 7.7
50/50	1741 ± 3.5
25/75	1686 ± 6.6
CREKA/DTPA-BSA(Gd)	
100/0	2398 ± 25.8
75/25	1114 ± 10.2
50/50	755.8 ± 7.8
25/75	1471 ± 22.3
NT/DTPA-BSA(Gd)	
100/0	2398 ± 20.9
75/25	1022 ± 7.9
50/50	551 ± 5.9
25/75	674 ± 7.3
phosphate-buffered saline (PBS)	2534 ± 11.4

Plaque Targeting of Clots in Vitro and in Atherosclerotic Mice. The fibrin-targeting ability of various CREKA-PAM formulations was first investigated using an in vitro clot-binding assay (Figure 2). Fibrin-containing clots were formed by incubating human plasma with thrombin. After polymerization, the clots were incubated with CREKA/DSPE-PEG2000-DTPA(Gd), NT/DSPE-PEG2000-DTPA(Gd), CREKA/DTPA-BSA(Gd), or NT/DTPA-BSA(Gd). After 1 h, clots were washed with PBS, digested with nitric acid, and Gd ions quantified by inductively coupled plasma mass spectrometry (ICP-MS). Whereas CREKA-targeting and NT micelles consisting of DTPA-BSA(Gd) did not have any significant binding differences, CREKA/DSPE-PEG2000-DTPA(Gd) formulations showed over 8-fold greater binding compared with their NT counterparts (Figure 2B). The higher binding of CREKA/DSPE-PEG2000-DTPA(Gd) could be explained by a more uniform mixture of the DSPE-PEG2000-CREKA (or NT) and DSPE-PEG2000-DTPA(Gd) molecules within the micelle versus the DTPA-BSA(Gd)-based micelles, where shape heterogeneity as well as the contrast provided by the Gd in the electron micrographs varied (Figure 1). As cylindrical micelles appeared lighter, this may indicate less overall Gd but more CREKA PA incorporation, which could contribute to an overall lower Gd measurement even if micelles targeted to a large extent. Further studies will design amphiphiles with both the targeting peptide and the chelating molecule into one amphiphile to interrogate this phenomenon.[29] Moreover, electrostatic interactions may contribute to fibrin binding of DTPA-BSA(Gd) micelles; controls scrambling the CREKA sequence or mutating the sequence (E → D and K → R) will be used to validate specificity of targeting in future studies.

DOI: 10.1021/acsomega.6b00210
ACS Omega 2016, 1, 996−1003

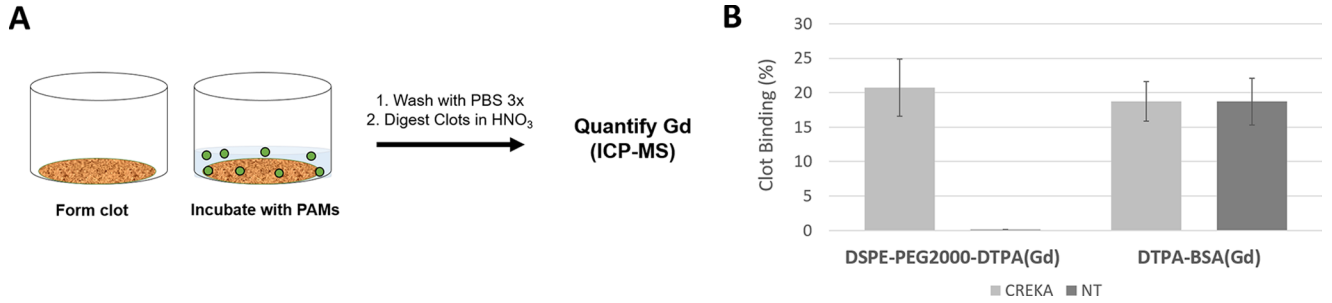

Figure 2. Schematic of (A) clot-binding assay and (B) quantification of micelle binding to clots in vitro by ICP-MS.

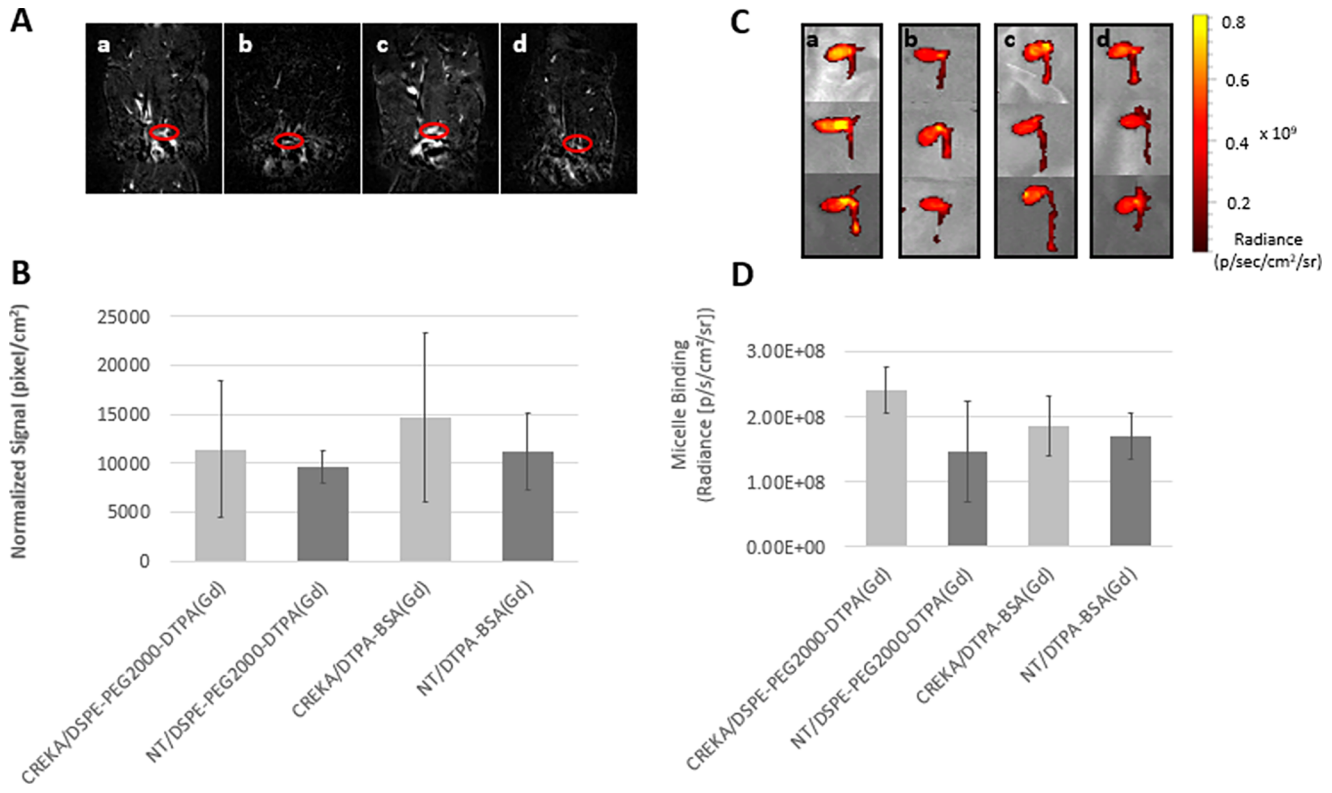

Figure 3. MR images of the (A) contrast-enhanced aortic arches (red oval) via micelles (a—CREKA/DSPE-PEG2000-DTPA(Gd); b—NT/DSPE-PEG2000-DTPA(Gd); c—CREKA/DTPA-BSA(Gd); d—NT/DTPA-BSA(Gd)). (B) Quantification of MR signal. (C) cy7 signal of hearts and aortas via optical imaging. (D) Quantification of cy7 signal (average flux) approximately 1 h after micelle administration.

Next, the targeting ability of nanoparticles was tested in vivo using the ApoE KO mouse (Figure 3). ApoE KO mice are homozygous for the Apoe^{tm1Unc} mutation and show an increase in total plasma cholesterol levels, lesions by 3 months, and can be induced with advanced stages of atherosclerosis using a Western diet.[30] Three-month-old mice were fed a high-fat diet for 3 months, and nanoparticle formulations were administered intravenously before *T*1-weighted MRI of the aorta, approximately 1 h after micelle injection; the addition of gadolinium increases the *T*1 relaxation rate of nearby water protons, providing positive contrast or a bright signal. Unlike the in vitro binding assay, coronal scans of the aortic arch showed an increased in contrast of CREKA micelles consisting of either DSPE-PEG2000-DTPA(Gd) or DTPA-BSA(Gd) compared to their NT micelle counterparts (Figure 3A). These results were further confirmed via quantification, although no statistical differences were found (Figure 3B). However, in addition to *T*1-weighted imaging, future *T*2-weighted and proton-density-weighted imaging may further discriminate plaque anatomy and composition and provide additional insights into targeting and imaging potential of CREKA micelles. Next, hearts and the aortas were excised and imaged using optical imaging, and the average photon flux was quantified (Figure 3C,D). Similarly, CREKA micelles consisting of either DSPE-PEG2000-DTPA-(Gd) or DTPA-BSA(Gd) had increased fluorescence signal (CREKA vs NT DSPE-PEG2000-DTPA(Gd) 2.4×10^8 vs 1.5×10^8 and CREKA vs NT DTPA-BSA(Gd) 1.9×10^8 vs 1.7×10^8 p/s/cm^2/sr). This was also the case for total flux (Figure S5). These differences between in vitro and in vivo targeting confirm the importance of animal studies, and one explanation could be the presence of a protein corona upon adsorbing components in plasma, neutralizing the targeting advantage and benefits found in vitro.[31,32] Future studies varying PEG length of the different PAs will be useful in reducing nonspecific protein adsorption and optimizing clot-binding and uptake. Figure S6 nonetheless shows immunohistochemistry staining of fibrin present within the aorta.

DOI: 10.1021/acsomega.6b00210
ACS Omega 2016, 1, 996−1003

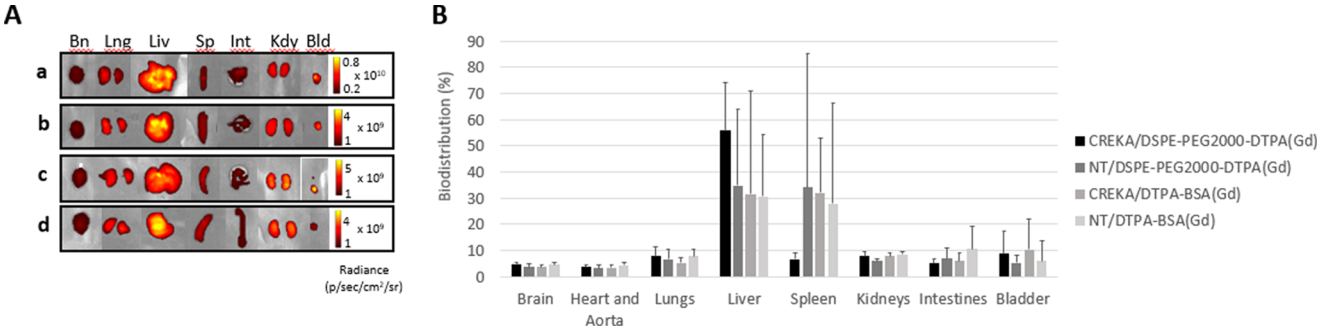

Figure 4. Biodistribution of micelles (a—CREKA/DSPE-PEG2000-DTPA(Gd), b—NT/DSPE-PEG2000-DTPA(Gd), c—CREKA/DTPA-BSA(Gd), d—NT/DTPA-BSA(Gd)) 90 min postinjection represented via (A) optical imaging and (B) quantification of the cy7 signal.

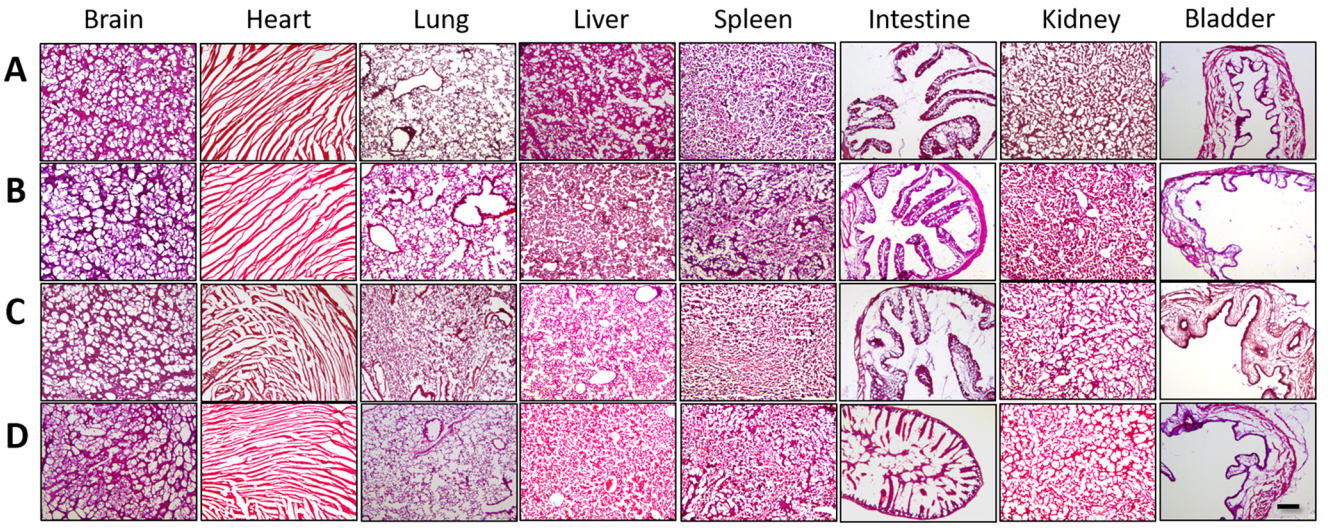

Figure 5. H and E staining of major organs after (A) CREKA/DSPE-PEG2000-DTPA(Gd), (B) NT/DSPE-PEG2000-DTPA(Gd), (C) CREKA/DTPA-BSA(Gd), and (D) NT/DTPA-BSA(Gd) administration. SB: 250 μm.

Biodistribution and Histology. Figure 4A provides biodistribution of nanoparticles throughout the brain, lung, liver, spleen, intestines, kidney, and bladder after approximately 90 min postinjection using optical imaging. All micelles primarily accumulated in the liver and the spleen with a moderate amount of uptake found within the kidneys and bladder as compared to the rest of the organs (Figure 4B). This is consistent with previous findings demonstrating that micelles are cleared through renal excretion as well as the monocyte phagocytic system (MPS, also called the reticuloendothelial system or RES).[12] Our micelles are on the smaller end of nanoparticle size, which render them capable of both glomerular filtration by the kidneys and elimination by macrophages via MPS.[33−35] As micelles are self-assembling and dynamic nanoparticles, it is also possible that some amphiphilic monomers bind with the target and cause micelle disassembly. As a result, nonbound monomers are cleared through the bladder. This process would likely occur multiple times as particles are recirculated throughout the body, ultimately saturating the target sites and diluting the particle concentration below the CMC. The ability for our nanoparticles to (1) target and image diseased tissues and (2) be cleared in a timely and appropriate manner may be an advantage as a diagnostic system, particularly to those patients undergoing recurring imaging sessions; this is in contrast to current MRI agents in which deposits found in the brain have triggered investigations regarding their safety.[36] Future studies interrogating the targeting and clearance properties of dynamic versus crosslinked particles versus monomers will help further tailor our design for diagnostic versus therapeutic applications that require varying half-lives and clearance properties. Previous studies showed that over 90% of micelles are cleared by 7 days.[37]

Histopathological evaluation of major organs, including kidneys, spleen, and liver, using hematoxylin and eosin staining showed no signs of cellular or tissue damage and did not detect abnormal lesions upon administration of any micelle type (Figure 5). Tissue morphology was comparable to organ structures obtained from mice injected with PBS, confirming the safety of these micelles as MRI contrast agents. This is consistent with previous in vitro data assessing biocompatibility of Gd-incorporated PAMs via Live/Dead assay. Altogether, fibrin-binding micelles as contrast-enhancing agents for atherosclerosis was demonstrated in vivo. Longer time points and additional animal studies will further delineate the full potential of targeting and enhancement, duration of signal enhancement, as well as clearance rate in future studies.

CONCLUSIONS

In this study, we designed micelle-based diagnostic agents for imaging fibrin-containing atherosclerotic plaques in vivo, and the potential of targeting plaques and dual, optical imaging−MRI was provided. Fibrin targeting was demonstrated by incorporating CREKA PAs with various Gd-chelating mole-

DOI: 10.1021/acsomega.6b00210
ACS Omega 2016, 1, 996−1003

cules, and the resulting micelle was characterized. Whereas in vitro studies confirmed that a uniform amphiphile backbone and micelle shape homogeneity had a large contribution to the clot-targeting capability, in vivo studies showed fibrin specificity was conferred by the peptide ligand without much difference between the nanoparticle formulations. Larger animal experiments will further interrogate the binding differences between the nanoparticle types in future studies. Despite the high level of mortality, the cardiovascular field has not benefited to a similar degree as cancer from recent advances in nanomedicine. Applications of medical nanotechnology toward cancer far outnumber those to cardiovascular disease by orders of magnitude. Similarly to cancer applications, nanomedicine can bring numerous powerful advantages, including early detection by amplification of small signals, local delivery of diagnostic contrast agents and therapeutics, and simultaneous delivery of a battery of agents. Our study that incorporates and compares fibrin-targeting micelles containing Gd-chelators can expand nanoparticle use in cardiovascular diseases and will lay the groundwork for targeted delivery of micelles for the detection of thrombosis via contrast-enhancing agents and concurrent therapeutic delivery for theranostic applications.

MATERIALS AND METHODS

Synthesis and Construction of Micelles. CREKA [Cys-Arg-Glu-Lys-Ala] peptides were synthesized via Fmoc-mediated solid-phase peptide synthesis methods using an automated PS3 Benchtop Peptide Synthesizer (Protein Technologies, Tucson, AZ) on rink Amide resin (Anaspec, Fremont, CA), as previously described.[37] CREKA peptides were cleaved and deprotected with 94:2.5:2.5:1 by volume trifluoroacetic acid (TFA)/1,2-ethanedithiol/H_2O/triisopropylsilane, dissolved in water, lyophilized, and stored as powders at 20 °C until use. Peptides were purified by reverse-phase high-performance liquid chromatography (HPLC) (Prominence, Shimadzu, Columbia, MD) on a C8 column (Waters, Milford, MA) at 50 °C using 0.1% TFA in acetonitrile/water mixtures and characterized by MALDI-TOF/TOF mass spectral analysis (Biflex III; Bruker, Billerica, MA). CREKA peptides were conjugated via a thioether linkage to DSPE-PEG(2000)-maleimide (Avanti Polar Lipids, Alabaster, AL) via the cysteine. After reaction at room temperature (RT) for 24 h, the PAs were purified and characterized as described above.

Gadolinium (Gd)-containing DSPE-PEG(2000) amphiphiles were synthesized by reacting DTPA-tetra (Macrocyclics, Dallas, TX) to DSPE-PEG(2000)-amine (Avanti Polar Lipids) in 1:1 molar ratio in dimethylformamide via a peptide bond. DSPE-PEG2000-DTPA-tetra was precipitated and purified as described above. The *tert*-butyl protecting groups were removed in 12 M HCl for 2 h before pH neutralization and purification via HPLC (C4 column). Gd ions were chelated onto the amphiphile by adding Gd(Cl_3) (Sigma Aldrich, St. Louis, MO) in a 1:1 molar ratio in 0.5 M sodium acetate (pH 5.5) for 1 h, and free Gd ions were separated by a PD-10 desalting column (GE Healthcare Life Sciences, Pittsburgh, PA). All amphiphiles in this study were characterized by MALDI-TOF/TOF mass spectral analysis (Biflex III, Bruker, Billerica, MA).

Cy7 mono-*N*-hydroxysuccinimide ester (GE Healthcare Life Sciences, Pittsburgh, PA, USA) was covalently attached to DSPE-PEG(2000)-amine by an amide bond to form fluorescently labeled amphiphiles. Molecules were dissolved in 10 mM aqueous sodium carbonate buffer (pH 8.5) and after 24 h of reaction, the mixture was purified on a C4 column and characterized by HPLC and MS as described above.

DSPE-PEG(2000)-DTPA(Gd)-containing PAMs were constructed by dissolving DSPE-PEG(2000)-CREKA, DSPE-PEG(2000)-cy7, and DSPE-PEG(2000)-DTPA(Gd) in methanol, mixing the components, and evaporating the mixture under nitrogen gas. The resulting film was dried under vacuum, and hydrated at 70 °C for 60 min in PBS under sonication, and allowed to cool to RT. Control, NT-Gd PAMs were self-assembled by using DSPE-PEG(2000)-OCH_3. CREKA-PAMs consisting of commercially available Gd-chelators were assembled by adding DTPA-bis(stearylamide)(Gd) (DTPA-BSA(Gd)) or DSPE-DTPA(Gd) (Avanti Polar Lipids, Alabaster, AL).

Micelle Characterization. Micelle samples for TEM were prepared by placing 6 μL of 50 μM of nanoparticle solution on 400 mesh lacey carbon grids (Ted Pella, Redding, CA) for 5 min. Excess liquid was wicked away with filter paper and the grid was washed with Milli-Q water. Dried samples were imaged on a JEOL 1230 TEM (JEOL, Ltd., Tokyo, Japan).

A total of 500 μM micelle solutions consisting of DSPE-PEG(2000)-CREKA or DSPE-PEG2000-OCH_3 with DSPE-PEG(2000)-DTPA(Gd) or DTPA-BSA(Gd) (1:1) were assessed by DLS. DLS measurements were determined at 90° and 637 nm using a Brookhaven Instruments (Holtzville, NY) system consisting of a BI-200SM goniometer and a BI-9000AT autocorrelator.

The *T*1 relaxation times of micelles were measured at 1.5 T Philips Achieva scanner (Philips, Healthcare, Best, The Netherlands). *T*1 longitudinal relaxation times were measured using vials containing 100 μM PAMs with varied ratios of DSPE-PEG(2000)-CREKA and DSPE-PEG(2000)-DTPA(Gd) or DTPA-BSA(Gd). The *T*1-mapping sequence consisted of a fast spin echo inversion recovery (FSE-IR) with varying inversion times (TIs). The FSE-IR acquisition parameters were as follows: TR = 12 s; TE = 15 ms; TI = 50, 100, 250, 500, 750, 1000, 2000, 3000, 4000, 5000 ms; acquisition voxel size of 1 mm × 1 mm and 5 mm slice thickness. Software written in Matlab (MathWorks, Natick, MA) was used to analyze data. The FSE-IR images were fit, using a nonlinear least squares fitting algorithm, on a voxel-by-voxel basis to the signal model (eq 1)

$$M(\mathrm{TI}) = M_o(1 - 2\,e^{-\mathrm{TI}/T1} + e^{-\mathrm{TR}/T1}) \quad (1)$$

where M(TI) is the measured signal at each TI and M_o is the equilibrium magnetization. These fits provided a *T*1 value for each voxel. Regions of interest (ROI) within vials were used to calculate the average *T*1 values of PAMs. ROIs had a cross-sectional diameter of 9 mm in the acquisition plane, in the calculated *T*1 maps.

Clot Binding of Micelles in Vitro. To test targeting ability of CREKA-PAMs, fibrin-containing clots were made according to established methods.[38] Specifically, 225 μL of human plasma (Sigma Aldrich, St. Louis, MO) was diluted in 75 μL of 100 mM $CaCl_2$ before adding 5 units of thrombin. After 5 min, clots were incubated with 500 μM PAMs for 1 h, washed with PBS 3 times, and digested in nitric acid. PAM binding was quantified by measuring Gd ions via ICP-MS (Agilent, Santa Clara, CA).

MRI of Atherosclerosis in a Murine Model. Female, 12 week old, transgenic mice homozygous for the *Apoe*^{tm1Unc} mutation (The Jackson Laboratory, Bar Harbor, ME) were fed a high-fat diet that consists of 21% (w/w) fat, 0.15% (w/w) cholesterol, 19.5% (w/w) casein, and no sodium cholate

DOI: 10.1021/acsomega.6b00210
ACS Omega 2016, 1, 996−1003

(Harlan, Indianapolis, IN) for 12 weeks to generate plaques.[39] All animals were anesthesized using isoflurane and underwent a preinjection baseline, MR scan (coronal plane) and reference images were obtained via *T*2-weighted spin echo (repetition time/echo time: 4000/20 ms; rare factor: 4, sinc3 pulse 450 μs, excitation/refocusing flip angle: 90/180°; field of view (FOV): 2.56 × 2.56 cm^2, slice thickness: 500 μm, resolution: 100 μm^2) at the Lynn S. Florsheim MRIS Lab at the University of Chicago.[40−43] CREKA or NT micelles with either DSPE-PEG(2000)-DTPA(Gd) or DTPA-BSA(Gd) (45:45:10 mol % Gd/PA/cy7 amphiphile, 400 μL, 1 mM in PBS, $N \geq 3$) were injected intravenously via a tail-vein catheter. Immediately after micelle administration, MRI scans of the aorta were performed using TOF (repetition time/echo time: 10.9/1.75 ms; flip angle: 60°; FOV: 2.56 × 2.56 cm^2, slice thickness: 500 μm, resolution: 100 μm^2) and lasted approximately 90 min. An inflow saturation band of 3 mm was used with a slice gap of 3 mm for additional luminal flow suppression, and a saturation pulse was used to eliminate background signal and minimize chemical shift artifacts. Imaging slices were matched to precontrast images and background subtracted using ImageJ software. To quantify the MRI results, the signal of the aortic arch was normalized by the muscle signal and signal intensity measurements of ROIs was quantified via ImageJ. All animal studies were conducted in accordance with NIH guidelines and were approved by the University of Chicago's IACUC (Chicago, IL).

Biodistribution and Histological Assessment. After optical imaging and euthanasia, the brain, heart, aorta, lung, intestines, liver, kidney, spleen, and bladder were collected for biodistribution and histological assessment. Near-infrared fluorescence imaging was conducted using an IVIS 200 and fluorescence signal quantified via Living Image software (Perkin Elmer, Downers Grove, IL). Organs were fixed with 4% paraformaldehyde overnight at 4 °C. Tissues were placed in a solution of 30% sucrose for 8 h and frozen in OCT (Tissue Tek, Sakura Finetek, Torrance, CA). Samples were then cryosectioned via a cryostat (Microm HM 525, Fisher Scientific, Pittsburgh, PA), and 5−7 μm sectioned were stained with hemotoxylin and eosin (H and E), and imaged (DMI6000 B, Leica Microsystems, Inc., Buffalo Grove, IL). Images provided are representative sections.

To assess fibrin expression, mouse, rabbit, anti-mouse fibrinogen α was used on aortic sections (1:200, Santa Cruz Biotechnology, Santa Cruz, CA, sc-33580). Secondary antibodies included biotinylated rabbit anti-mouse antibody (1:200, 10 μg/mL, Vector Laboratories, Burlingame, CA, BA-1000) and antigen−antibody binding was detected by the Elite standard Vectastain ABC kit (PK-6100; Vector Laboratories) and DAB (K3468; DAKO, Carpinteria, CA) system.

Statistical Analysis. Student's *t*-tests were used to compare two groups, whereas analysis of variance using Newman−Keuls multiple comparison test post-hoc analysis determined significant differences among three or more groups. A *p*-value of ≤0.05 was considered to be significant. Data are expressed as mean ± SD or SEM.

■ ASSOCIATED CONTENT

Supporting Information

The Supporting Information is available free of charge on the ACS Publications website at DOI: 10.1021/acsomega.6b00210.

MALDI/TOF mass spectrometry results; TEM images; DLS data; in vivo fluorescence data; representative immunohistochemistry data (Figures S1−S6) (PDF)

■ AUTHOR INFORMATION

Corresponding Author

*E-mail: eunchung@usc.edu. Tel: +1-213-740-2925. Fax: +1-213-821-3897.

ORCID

John C. Barrett: 0000-0002-1113-1351

Eun Ji Chung: 0000-0002-7726-5555

Present Address

∥Department of Biomedical Engineering, University of Southern California, 1042 Downey Way, Los Angeles, California 90089-1111, United States (C.P.) (E.J.C.).

Notes

The authors declare no competing financial interest.

■ ACKNOWLEDGMENTS

The authors would like to acknowledge the MRIS Facility at the University of Chicago for the experimental and intellectual support regarding the MRI studies, and the National Heart, Lung, and Blood Institute (NHLBI), K99HL124279, granted to EJC.

■ REFERENCES

(1) Mozaffarian, D.; Benjamin, E. J.; Go, A. S.; Arnett, D. K.; Blaha, M. J.; Cushman, M.; de Ferranti, S.; Després, J.-P.; Fullerton, H. J.; Howard, V. J.; Huffman, M. D.; Judd, S. E.; Kissela, B. M.; Lackland, D. T.; Lichtman, J. H.; Lisabeth, L. D.; Liu, S.; Mackey, R. H.; Matchar, D. B.; McGuire, D. K.; Mohler, E. R.; Moy, C. S.; Muntner, P.; Mussolino, M. E.; Nasir, K.; Neumar, R. W.; Nichol, G.; Palaniappan, L.; Pandey, D. K.; Reeves, M. J.; Rodriguez, C. J.; Sorlie, P. D.; Stein, J.; Towfighi, A.; Turan, T. N.; Virani, S. S.; Willey, J. Z.; Woo, D.; Yeh, R. W.; Turner, M. B. Heart Disease and Stroke Statistics—2015 Update: A Report From the American Heart Association. *Circulation* **2015**, *131*, No. e29.

(2) NHLBI. What is atherosclerosis? http://www.nhlbi.nih.gov/health/health-topics/topics/atherosclerosis (accessed Oct 30, 2015).

(3) Staff, M. C. Arteriosclerosis/atherosclerosis. http://www.mayoclinic.org/diseases-conditions/arteriosclerosis-atherosclerosis/diagnosis-treatment/research/rsc-20167164 (accessed Oct 30, 2015).

(4) American Heart Association. What is Cardiovascular Disease?, 2016. http://www.heart.org/HEARTORG/Caregiver/Resources/WhatisCardiovascularDisease/What-is-Cardiovascular-Disease_UCM_301852_Article.jsp#.V_XWT9orI2w.

(5) Otsuka, F.; Nakano, M.; Kolodgie, F. D.; Virmani, R., Evaluation of Vulnerable Atherosclerotic Plaques. In *Coronary Artery Disease*; Willerson, T. J., Holmes, J. R. D., Eds.; Springer: London, 2015; pp 409−419.

(6) Briley-Saebo, K. C.; Mulder, W. J. M.; Mani, V.; Hyafil, F.; Amirbekian, V.; Aguinaldo, J. G. S.; Fisher, E. A.; Fayad, Z. A. Magnetic resonance imaging of vulnerable atherosclerotic plaques: Current imaging strategies and molecular imaging probes. *J. Magn. Reson. Imaging* **2007**, *26*, 460−479.

(7) Chung, E. J.; Tirrell, M. Recent Advances in Targeted, Self-Assembling Nanoparticles to Address Vascular Damage Due to Atherosclerosis. *Adv. Healthcare Mater.* **2015**, *4*, 2408−2422.

(8) Hartgerink, J. D.; Beniash, E.; Stupp, S. I. Self-assembly and mineralization of peptide-amphiphile nanofibers. *Science* **2001**, *294*, 1684−1688.

(9) Akerman, M. E.; Chan, W. C. W.; Laakkonen, P.; Bhatia, S. N.; Ruoslahti, E. Nanocrystal targeting in vivo. *Proc. Natl. Acad. Sci. U.S.A.* **2002**, *99*, 12617−12621.

DOI: 10.1021/acsomega.6b00210
ACS Omega 2016, 1, 996−1003

(10) Chung, E. J. Targeting and therapeutic peptides in nanomedicine for atherosclerosis. *Exp. Biol. Med.* **2016**, *241*, 891−898.
(11) Peters, D.; Kastantin, M.; Kotamraju, V. R.; Karmali, P. P.; Gujraty, K.; Tirrell, M.; Ruoslahti, E. Targeting atherosclerosis by using modular, multifunctional micelles. *Proc. Natl. Acad. Sci. U.S.A.* **2009**, *106*, 9815−9819.
(12) Chung, E. J.; Mlinar, L. B.; Sugimoto, M. J.; Nord, K.; Roman, B. B.; Tirrell, M. In vivo biodistribution and clearance of peptide amphiphile micelles. *Nanomedicine* **2015**, *11*, 479−487.
(13) Kuo, C.-H.; Leon, L.; Chung, E. J.; Huang, R.-T.; Sontag, T. J.; Reardon, C. A.; Getz, G. S.; Tirrell, M.; Fang, Y. Inhibition of atherosclerosis-promoting microRNAs via targeted polyelectrolyte complex micelles. *J. Mater. Chem. B* **2014**, *2*, 8142−8153.
(14) Chung, E. J.; Pineda, F.; Nord, K.; Karczmar, G.; Lee, S.-K.; Tirrell, M. Fibrin-targeting, peptide amphiphile micelles as contrast agents for molecular MRI. *J. Cell Sci. Ther.* **2014**, *5*, 181.
(15) Mallat, Z.; Tedgui, A. Current Perspective on the Role of Apoptosis in Atherothrombotic Disease. *Circ. Res.* **2001**, *88*, 998−1003.
(16) Cui, H.; Webber, M. J.; Stupp, S. I. Self-Assembly of Peptide Amphiphiles: From Molecules to Nanostructures to Biomaterials. *Biopolymers* **2010**, *94*, 1−18.
(17) Trent, A.; Marullo, R.; Lin, B.; Black, M.; Tirrell, M. Structural properties of soluble peptide amphiphile micelles. *Soft Matter* **2011**, *7*, 9572−9582.
(18) Bisht, S.; Feldmann, G.; Koorstra, J.-B. M.; Mullendore, M.; Alvarez, H.; Karikari, C.; Rudek, M. A.; Lee, C. K.; Maitra, A.; Maitra, A. In vivo characterization of a polymeric nanoparticle platform with potential oral drug delivery capabilities. *Mol. Cancer Ther.* **2008**, *7*, 3878−3888.
(19) Mlinar, L. B.; Chung, E. J.; Wonder, E. A.; Tirrell, M. Active targeting of early and mid-stage atherosclerotic plaques using self-assembled peptide amphiphile micelles. *Biomaterials* **2014**, *35*, 8678−8686.
(20) Chung, E. J.; Mlinar, L. B.; Nord, K.; Sugimoto, M. J.; Wonder, E.; Alenghat, F. J.; Fang, Y.; Tirrell, M. Monocyte-Targeting Supramolecular Micellar Assemblies: A Molecular Diagnostic Tool for Atherosclerosis. *Adv. Healthcare Mater.* **2015**, *4*, 367−376.
(21) Karmali, P. P.; Kotamraju, V. R.; Kastantin, M.; Black, M.; Missirlis, D.; Tirrell, M.; Ruoslahti, E. Targeting of albumin-embedded paclitaxel nanoparticles to tumors. *Nanomedicine* **2009**, *5*, 73−82.
(22) FDA. Drug Safety Communication: FDA evaluating the risk of brain deposits with repeated use of gadolinium-based contrast agents for magnetic resonance imaging (MRI). http://www.fda.gov/Drugs/DrugSafety/ucm455386.htm.
(23) Beilvert, A.; Cormode, D. P.; Chaubet, F.; Briley-Saebo, K. C.; Mani, V.; Mulder, W. J. M.; Vucic, E.; Toussaint, J.-F.; Letourneur, D.; Fayad, Z. A. A tyrosine PEG-micelle magnetic resonance contrast agent for the detection of lipid rich areas in atherosclerotic plaque. *Magn. Reson. Med.* **2009**, *62*, 1195−1201.
(24) Zhou, Z.; Lu, Z.-R. Gadolinium-Based Contrast Agents for MR Cancer Imaging. *Wiley Interdiscip. Rev.: Nanomed. Nanobiotechnol.* **2013**, *5*, 1−18.
(25) Langereis, S.; de Lussanet, Q. G.; van Genderen, M. H. P.; Backes, W. H.; Meijer, E. W. Multivalent Contrast Agents Based on Gadolinium−Diethylenetriaminepentaacetic Acid-Terminated Poly(propylene imine) Dendrimers for Magnetic Resonance Imaging. *Macromolecules* **2004**, *37*, 3084−3091.
(26) Grant, C. W. M.; Karlik, S.; Florio, E. A liposomal MRI contrast agent: Phosphatidylethanolamine-DTPA. *Magn. Reson. Med.* **1989**, *11*, 236−243.
(27) Grant, C. W. M.; Barber, K. R.; Florio, E.; Karlik, S. A phospholipid spin label used as a liposome-associated MRI contrast agent. *Magn. Reson. Med.* **1987**, *5*, 371−376.
(28) Hu, H. H.; Nayak, K. S. Change in the proton T1 of fat and water in mixture. *Magn. Reson. Med.* **2010**, *63*, 494−501.
(29) Chan, L. W.; White, N. J.; Pun, S. H. Synthetic Strategies for Engineering Intravenous Hemostats. *Bioconjugate Chem.* **2015**, *26*, 1224−1236.
(30) Reardon, C. A.; Getz, G. S. Mouse models of atherosclerosis. *Curr. Opin. Lipidol.* **2001**, *12*, 167−173.
(31) Monopoli, M. P.; Walczyk, D.; Campbell, A.; Elia, G.; Lynch, I.; Baldelli Bombelli, F.; Dawson, K. A. Physical−Chemical Aspects of Protein Corona: Relevance to in Vitro and in Vivo Biological Impacts of Nanoparticles. *J. Am. Chem. Soc.* **2011**, *133*, 2525−2534.
(32) Nel, A. E.; Madler, L.; Velegol, D.; Xia, T.; Hoek, E. M. V.; Somasundaran, P.; Klaessig, F.; Castranova, V.; Thompson, M. Understanding biophysicochemical interactions at the nano−bio interface. *Nat. Mater.* **2009**, *8*, 543−557.
(33) Deen, W. M.; Lazzara, M. J.; Myers, B. D. Structural determinants of glomerular permeability. *Am. J. Physiol.* **2001**, *281*, F579−F596.
(34) Longmire, M.; Choyke, P. L.; Kobayashi, H. Clearance properties of nano-sized particles and molecules as imaging agents: considerations and caveats. *Nanomedicine* **2008**, *3*, 703−717.
(35) Choi, H. S.; Liu, W.; Misra, P.; Tanaka, E.; Zimmer, J. P.; Ipe, B. I.; Bawendi, M. G.; Frangioni, J. V. Renal clearance of quantum dots. *Nat. Biotechnol.* **2007**, *25*, 1165−1170.
(36) Malayeri, A. A.; Brooks, K. M.; Bryant, L. H.; Evers, R.; Kumar, P.; Reich, D. S.; Bluemke, D. A. National Institutes of Health perspective on reports of gadolinium deposition in the brain. *J. Am. Coll. Radiol.* **2016**, *13*, 237−241.
(37) Chung, E. J.; Cheng, Y.; Morshed, R.; Nord, K.; Han, Y.; Wegscheid, M. L.; Auffinger, B.; Wainwright, D. A.; Lesniak, M. S.; Tirrell, M. V. Fibrin-binding, peptide amphiphile micelles for targeting glioblastoma. *Biomaterials* **2014**, *35*, 1249−1256.
(38) Wen, A. M.; Wang, Y.; Jiang, K.; Hsu, G. C.; Gao, H.; Lee, K. L.; Yang, A. C.; Yu, X.; Simon, D. I.; Steinmetz, N. F. Shaping bio-inspired nanotechnologies to target thrombosis for dual optical-magnetic resonance imaging. *J. Mater. Chem. B* **2015**, *3*, 6037−6045.
(39) Whitman, S. C. A practical approach to using mice in atherosclerosis research. *Clin. Biochem. Rev.* **2004**, *25*, 81−93.
(40) Briley-Saebo, K. C.; Cho, Y. S.; Shaw, P. X.; Ryu, S. K.; Mani, V.; Dickson, S.; Izadmehr, E.; Green, S.; Fayad, Z. A.; Tsimikas, S. Targeted Iron Oxide Particles for In Vivo Magnetic Resonance Detection of Atherosclerotic Lesions With Antibodies Directed to Oxidation-Specific Epitopes. *J. Am. Coll. Cardiol.* **2011**, *57*, 337−347.
(41) van Tilborg, G. A. F.; Vucic, E.; Strijkers, G. J.; Cormode, D. P.; Mani, V.; Skajaa, T.; Reutelingsperger, C. P. M.; Fayad, Z. A.; Mulder, W. J. M.; Nicolay, K. Annexin A5-Functionalized Bimodal Nanoparticles for MRI and Fluorescence Imaging of Atherosclerotic Plaques. *Bioconjugate Chem.* **2010**, *21*, 1794−1803.
(42) Amirbekian, V.; Lipinski, M. J.; Briley-Saebo, K. C.; Amirbekian, S.; Aguinaldo, J. G. S.; Weinreb, D. B.; Vucic, E.; Frias, J. C.; Hyafil, F.; Mani, V.; Fisher, E. A.; Fayad, Z. A. Detecting and assessing macrophages in vivo to evaluate atherosclerosis noninvasively using molecular MRI. *Proc. Natl. Acad. Sci. U.S.A.* **2007**, *104*, 961−966.
(43) te Boekhorst, B. C.; Bovens, S. M.; van de Kolk, C. W. A.; Cramer, M. J. M.; Doevendans, P. A. F. M.; ten Hove, M.; van der Weerd, L.; Poelmann, R.; Strijkers, G. J.; Pasterkamp, G.; van Echteld, C. J. A. The time window of MRI of murine atherosclerotic plaques after administration of CB2 receptor targeted micelles: inter-scan variability and relation between plaque signal intensity increase and gadolinium content of inversion recovery prepared versus non-prepared fast spin echo. *NMR Biomed.* **2010**, *23*, 939−951.

DOI: 10.1021/acsomega.6b00210
ACS Omega 2016, 1, 996−1003